Compositional Dependence of Segmental Dynamics in a Miscible Polymer Blend

G.-C. Chung and J. A. Kornfield*

Chemical Engineering Department, California Institute of Technology, Pasadena, California 91125

S. D. Smith

Procter & Gamble, Cincinnati, Ohio 45239

Received May 19, 1994®

ABSTRACT: The segmental motion of each species in polyisoprene/poly(vinylethylene) (PI/PVE) miscible blends is studied at three different compositions using two-dimensional deuteron exchange NMR (2D ^{2}H NMR). The individual species exhibit widely different mean mobilities and broad mobility distributions near the glass transition of each blend. As the PVE content increases, both the difference in mean mobilities between the two species and the width of the mobility distribution for both components increase. The change in these two types of dynamic heterogeneity with PVE content appears to produce the anomalous broadening of the glass transition. The mean reorientational correlation times of each component can differ by 2 orders of magnitude under identical conditions. This difference can be described in terms of distinct effective glass transition temperatures, T_g*, for the two species. The separation between the two effective glass transition temperatures increases almost monotonically with PVE content, consistent with the more pronounced thermorheological complexity of blends rich in PVE. The individual T_g*'s also exhibit a different compositional dependence from that of the calorimetric T_g of the blend observed by differential scanning calorimetry (DSC). This behavior can give rise to the complex compositional dependence of individual mobilities, apparent when the mobilities are compared at the same $T - T_g$ with respect to the DSC T_g of the blend.

1. Introduction

Miscible polymer blends are of great practical interest because a range of useful materials can be produced by blending existing polymers. One important goal is to tailor the blend properties based on the known properties of their constituent polymers. The glass transition temperature and the width of the glass transition are important properties that control the applicable temperature ranges of miscible blends. Material processing can be facilitated by the modification of flow properties through blending. The diffusivities of the individual species, which affect the kinetics of mixing and phase separation, can also be controlled once the effect of blending on their mobilities is understood. In addition, the study of miscible blends provides valuable information on the role of intrinsic dynamic properties and intermolecular interactions in determining the dynamics of polymers in general. Specifically, by varying the composition of miscible blends, we can study the modification of chain dynamics due to changes in interchain dynamic constraints, while holding intramolecular structure fixed.

Indeed, blending significantly alters the dynamics of both components, often to the extent that the distinction between individual species can hardly be observed.[1] Recent studies, however, show that individual species can retain their distinct motional characteristics, even though their dynamics in blends are very different than in their pure states.[2,3] Similar changes of solvent dynamics in a dilute polymer solution have also been observed.[4] In a number of miscible blends, changes in component dynamics are manifested by an anomalously broad glass transition[5–7] and a complex temperature and composition dependence of viscoelastic properties.[8–10] We have recently shown that two types of dynamic heterogeneities in blends simultaneously contribute to these macroscopic phenomena: intrinsic differences in component mobilities and broadening of the mobility distribution for both species due to local compositional variation.[3] Although these observations clearly demonstrate the effect of neighboring chains on the component dynamics, little information is available regarding the compositional dependence of the component dynamics and its relationship to the macroscopic properties of blends.

Phenomenological models that predict the compositional dependence of the glass transition temperature, T_g, of miscible blends usually require a number of fitting parameters.[11–13] Moreover, these theories are not compatible with the distinct responses of constituent polymers, which suggests the possibility of two distinct effective glass transition temperatures. Likewise, theoretical predictions of the composition dependence of tracer diffusivities and ultimately monomeric friction coefficients of each species do not agree with the experimental observations.[10,14] It has been pointed out that this disagreement probably comes from the experimental difficulty of handling the composition-dependent glass transition temperature, $T_g(\phi)$.[15] Perhaps these discrepancies are related to more fundamental questions regarding the compositional dependence of segmental dynamics and the nature of cooperative dynamics underlying the glass transition.

Our objective in this paper is to provide experimental measurements of the segmental dynamics in miscible blends as a function of composition. To quantitatively characterize the dynamics of each species in blends, both selective deuterium labeling and 2D ^{2}H NMR are used. The dynamics of individual species are clearly resolved by selective deuterium labeling, while the mean and distribution width of segmental mobility are quantitatively determined using 2D ^{2}H NMR. The segmental reorientation motion of interest is known to be correlated with the glass transition.[16] Therefore, the results pertain directly to understanding the compositional dependence of the dynamics underlying the broad glass transition of miscible blends. Longer length scale dynamics manifested in the

® Abstract published in *Advance ACS Abstracts*, September 1, 1994.

0024-9297/94/2227-5729$04.50/0

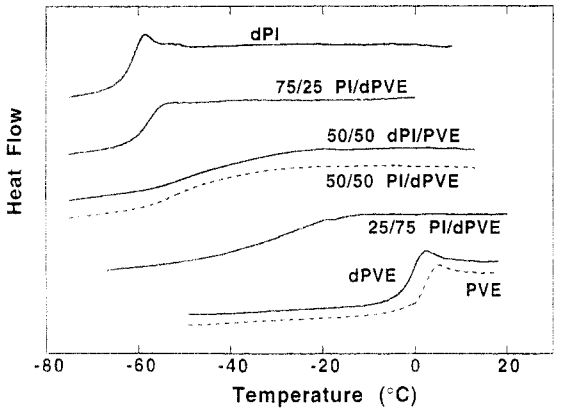

Figure 1. DSC traces for the homopolymers (PVE, dPVE, and dPI) and three PI/PVE blends (75/25 PI/PVE, 50/50 PI/PVE, and 25/75 PI/PVE).

viscoelastic and diffusion behavior at temperatures much above T_g are also related to these segmental motions. The exact nature of the latter relations, however, requires further knowledge of the way in which the heterogeneity in local segmental motion in the blend propagates out to the larger molecular scale represented by a Rouse segment.

In this work, blends of 1,4-polyisoprene (PI) and poly(vinylethylene) (PVE) (also known as 1,2-polybutadiene) are used as a model system. This pair is ideal for our study since it has been shown to be miscible in all proportions, yet has very weak interactions. Recent SANS experiments have shown that PI/PVE blends can be described by an interaction parameter, χ, which is small but negative at all accessible temperatures.[17] This is consistent with numerous previous studies,[18-20] which indicate that the blend is completely miscible without specific interaction. Furthermore, the identical DSC traces of PI/PVE blends and block copolymers of the same overall composition suggest that the broad glass transition in this blend is not due to concentration fluctuations associated with incipient phase separation, since such fluctuations would be much smaller in the block copolymer.[21] Therefore, this system can be modeled assuming random segmental mixing.

In the next section, our experimental approach is described. We then present the correlation time of segmental motion as a function of temperature and composition. The compositional dependence of segmental dynamics is discussed in terms of the effective glass transition, $T_{g,i}$*, for each species i. The effect of blending on the thermorheological complexity is also examined by comparing the mean correlation times with the monomeric friction coefficient, $\zeta_{0,i}$, obtained from the same set of blends. We then interpret our observations using a simple physical picture of the cooperative local segmental dynamics. We conclude with a brief summary of our findings.

2. Experimental Section

2.1. Materials. Four polymers are used in these experiments: hydrogenous and deuterio 1,4-polyisoprene (PI, dPI) and hydrogenous and deuterio poly(vinylethylene) (PVE, dPVE). All polymers are prepared by anionic synthesis and have narrow molecular weight distributions. Sample characterization has been reported previously.[3] The glass transitions of the blends and pure components are characterized by differential scanning calorimetry (DSC) (Figure 1).[22] The DSC traces were recorded for 25 mg samples at a heating rate of 10 °C/min, using a Perkin-Elmer System DSC-7. The pair of hydrogenous and deuterio PI's have essentially the same T_g, while the T_g of dPVE is about 2 K lower than the normal PVE, probably due to a small difference between their microstructures.[23] The blends containing deuterium-labeled species also show nearly identical DSC traces as the unlabeled counterparts. Due to mixed microstructure, the polymers are known not to crystallize.

For ^{2}H NMR measurements, we use deuterio homopolymers and matched pairs of dPI/PVE and PI/dPVE blends with PI weight fractions of 25, 50, and 75%. The blends are prepared by mixing 3 wt % toluene solutions of each component and slowly casting on a Teflon surface. The cast samples are dried at room temperature first under a hood and further under vacuum for more than a week. The blend samples are clear and free of bubbles, suggesting that the film is homogeneous and completely dried. No antioxidant is added to avoid possible effects on the local dynamics and T_g. The blend samples are subsequently sealed off under air in NMR sample tubes and kept in a freezer to retard oxidation.

2.2. Two-Dimensional Deuteron Exchange NMR. The segmental reorientation dynamics of polymers are studied near the glass transition using 2D ^{2}H exchange NMR.[24,25] The essence of this method is that the type and rate of segmental reorientation can be determined by analyzing the correlation of the deuteron resonance frequency before and after a controlled time period, t_m, called the mixing time.[24,25] The direct relationship between the segmental reorientation dynamics and the change in the deuteron magnetic resonance frequency arises from the fact that the resonance frequency, ω, depends directly on the orientation angle, θ, of the C–^{2}H bond with respect to the main magnetic field of the spectrometer. For the C–^{2}H bonds in dPI and dPVE, the electric field gradient at the deuterium nucleus is essentially uniaxial about the axis of the C–^{2}H bond. Therefore, the orientation dependence of the resonance frequency is approximately given by

$$\Delta\omega(\theta) = \frac{\delta}{2}[3\cos^2(\theta) - 1] \qquad (1)$$

where $\Delta\omega$ is the resonance frequency shift from the deuteron Larmor frequency ω_0; δ specifies the strength of the electric quadrupole coupling.[26] For the backbone C–^{2}H bond of rigid polymers, δ is about 125 kHz, while δ is reduced for the C–^{2}H bonds in a methyl rotor due to their fast motion about the threefold symmetry axis. Since ^{2}H is a spin $I = 1$ nucleus, two resonance frequency lines at $\omega^{\pm}(\theta) = \omega_0 \pm \Delta\omega(\theta)$ are associated with the ^{2}H on each C–^{2}H bond.

To quantify the correlation in resonance frequencies, ω_1 and ω_2, before and after the mixing time, we use a five-pulse 2D ^{2}H exchange NMR experiment.[27] The details of this experiment can be found elsewhere.[3,24,25,27] The five-pulse 2D exchange NMR sequence is built from three sets of pulses, constituting the evolution period, mixing period, and detection period. After the evolution period of time t_1, the amplitude of the nuclear spin magnetization is sinusoidally modulated with frequency ω_1 as dictated by the initial orientation of the C–^{2}H bond, θ_1. Reorientation may take place during the mixing time, t_m. For each value of t_1, the time-domain signal is recorded during the detection period as a function of time, t_2. As a function of t_2, this signal oscillates with $\omega_2 t_2$ as dictated by the final orientation, θ_2. The initial amplitude of this signal oscillates with $\omega_1 t_1$, as dictated by the initial angle θ_1.

When the range of times t_1 and t_2 ($\sim 2 \times 10^{-4}$ s) is short compared to the correlation time, τ_c, for reorientation of

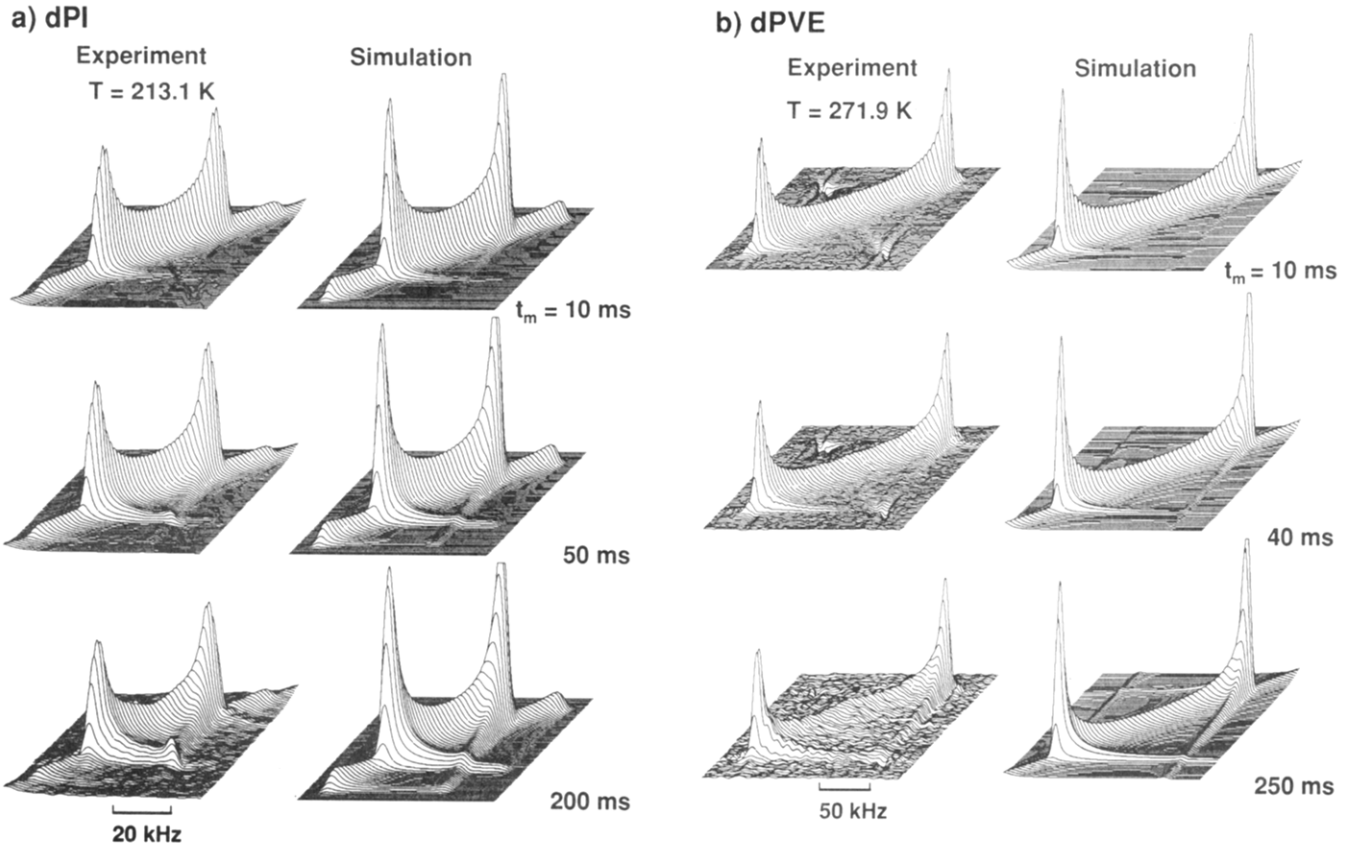

Figure 2. 2D ^{2}H exchange NMR spectra of two homopolymers, dPI and dPVE, obtained close to T_g, at 213.1 K (T_g + 2.7 K) and 271.8 K (T_g + 1.2 K), respectively. (a) Experimental and simulated spectra of dPI obtained with mixing times of 10, 50, and 200 ms. From the fit, we obtain a mean correlation time τ_{c_0} = 0.5 s and a width of the distribution σ = 1.25 decades. (b) Experimental and simulated spectra of dPVE obtained with mixing times of 10, 40, and 250 ms (τ_{c_0} = 1 s and σ = 1.0 decade).

C–^{2}H bonds, we can neglect reorientation during t_1 and t_2.[28–30] This is typically the case in amorphous polymers near T_g ($\tau_c \geq 10^{-3}$ s). However, when the reorientation is characterized by a very broad distribution of motional rates (3–5 decades), the above assumption may not be strictly valid.[28,30] In that case, while the mean motional rates lie in the slow motion regime, the fastest motions may lie in the intermediate dynamic range (1 μs $\leq \tau_c \leq$ 1 ms). Signals from the C–^{2}H bonds that have motional rates in this range are known to be significantly reduced due to incomplete refocusing of magnetization during the evolution and detection period.[28,30,31] The reduction of spectral intensity as a function of temperature, $R(T)$, can be characterized using the solid echo experiment.[33] Using the observed reduction, we develop an approximate scheme for correcting the apparent correlation time distribution determined from the 2D spectra for the correlation time dependent reduction. Since the loss of spectral intensity is maximized for $\tau_c \simeq 2/\delta$,[32] we can also obtain supplementary information about the temperature dependence of the mean correlation times.

All 2D spectra are recorded using a Bruker MSL 200 spectrometer equipped with a VT1000 temperature controller unit. A slightly modified Bruker broad-band wideline probe with a 7.5 mm coil is used. The 90° pulse length is 3.1 μs and a digitization rate of 3.2 μs is used to capture the complete range of the spectra along the t_1 and t_2 dimensions. The repetition time is varied from 300 ms to 1 s to obtain sufficiently relaxed spectra. Reasonable signal to noise is achieved with ~128 scans at the smallest mixing time and up to 1920 scans at the largest mixing time. The typical data size is 256 complex points along t_2 and 60 points along t_1. At each temperature, spectra are taken at three or more mixing times to probe the evolution of the reorientation distribution with time. The mixing time is varied from 0.5 to 400 ms, spanning almost 3 decades in time. The temperature is controlled to within ±0.5 K for each set of mixing times. The procedure we use to analyze the experimental spectra has been reported previously.[3]

3. Results

For both homopolymers, 2D spectra obtained very close to the DSC glass transition temperatures (T_g + 2.7 K for dPI and T_g + 1.2 K for dPVE) show similar degrees of reorientation at similar mixing times (Figure 2). The simulated spectra are obtained from the rotational diffusion model with a log-Gaussian distribution of correlation times. The log-mean correlation times determined by the fits shown in Figure 2 are 0.5 and 1 s for dPI (at T_g + 2.7 K) and dPVE (at T_g + 1.2 K), respectively. Some differences between the experimental and the simulated spectra are observed, particularly near the two diagonal peaks and their off-diagonal cross region. Such differences in the shape of 2D spectra between the experimental and the simulated spectra can arise from many origins not directly related to the reorientation dynamics, such as an anisotropic relaxation of magnetization during the mixing time, a small deviation from axial symmetry of the electric field gradient around the C–^{2}H bonds, and experimental imperfections. Since the degree of exchange sensitively affects how signal along the off-diagonal ridges changes relative to the diagonal intensity, the difference in appearance near the diagonal peaks and their off-diagonal cross region does not affect the accuracy of the fit parameters.

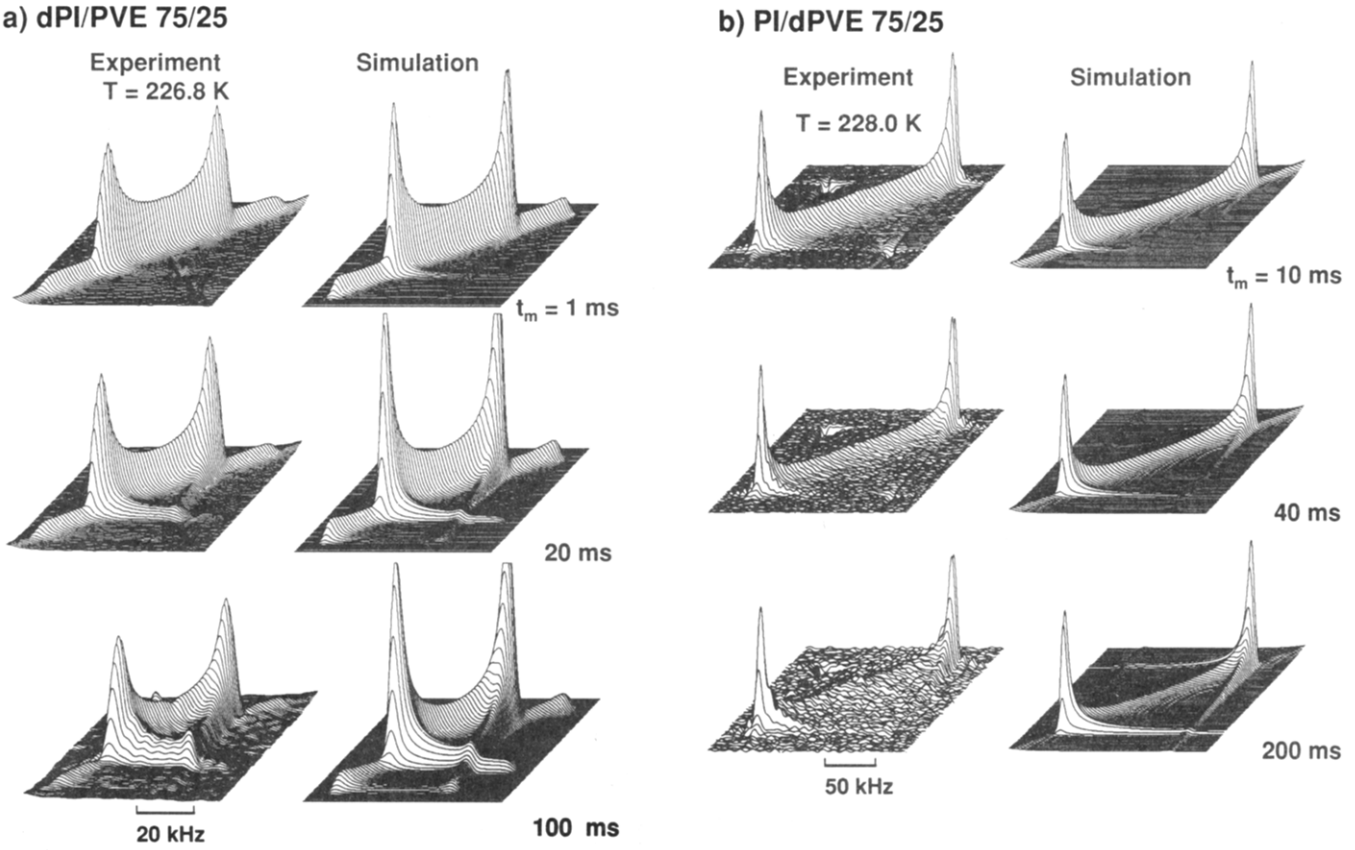

Figure 3. Experimental and simulated 2D ^{2}H exchange NMR spectra of the two components in 75/25 PI/PVE blends obtained at similar temperatures: (a) 75/25 dPI/PVE at 226.8 K (τ_{c_0} = 12.5 ms and σ = 1.35 decades); (b) 75/25 PI/dPVE at 228.0 K (τ_{c_0} = 0.5 s and σ = 1 decade).

In PI/PVE blends, the individual components have significantly different mobilities at all experimental temperatures, which is evidenced in the spectra obtained at nearly identical conditions (Figure 3). For the same blend composition and temperature, PI exhibits much faster reorientation than PVE. Direct inspection of the spectra in Figure 3 enables one to estimate the relative rates of PI and PVE motion and observe that they differ by more than a decade for both blend ratios. For example, in the 75/25 PI/PVE blends, the degree of exchange is more pronounced at a mixing time of 20 ms for dPI than for dPVE at a mixing time of 200 ms (Figure 3a,b).

To confirm that this stark difference in mobility is not an artifact of isotopic labeling, we have compared 2D ^{2}H exchange NMR spectra obtained from blends of the same overall composition but different fractions of labeled species. If deuterium labeling altered the phase behavior of these blends, changing the fraction of labeled chains would cause significant changes in the mobility of both species because the segmental mobility depends sensitively on the composition of neighboring chains. Instead, nearly identical exchange patterns are observed from 50/50 PI/PVE blends containing two different fractions of deuterated species (i.e., dPI spectra for 25:25/50 dPI:PI/PVE and 50/50 dPI/PI and dPVE spectra for 50/25:25 PI/dPVE:PVE and 50/50 PI/dPVE). This result suggests that deuteration does not observably affect the phase behavior of the blend, at least close to the glass transition as studied here.[35]

For the 25/75 PI/PVE blends, the dPI spectra exhibit a smeared out appearance, which indicates a significant fraction of segments have motional rates that fall in the intermediate dynamic regime (Figure 4a). The evidence of highly mobile PI units is observed even at temperatures where the motion of PVE is so slow that 2D spectra for 25/75 PI/dPVE do not show significant exchange intensities (e.g., 250 K). In fact, the dPI spectra obtained at a temperature 5 K higher than in Figure 4a exhibit not only a strongly smeared off-diagonal intensity but also asymmetrically distorted spectra with an isotropic peak at the center. These features have previously been observed in spectra obtained in the middle of the intermediate dynamic regime.[30]

The log-mean correlation time, τ_{c_0}, and the width of the correlation time distribution, σ, are determined by fitting the series of experimental spectra at each temperature with calculated spectra. In contrast to polystyrene (PS) and poly(2,6-dimethylphenylene oxide) (PXE) in PS/PXE blends,[2] whose 2D spectra have been interpreted in terms of a bimodal distribution of correlation times for each species, our experimental spectra of PI/PVE blends are consistent with a unimodal distribution of correlation times at all compositions. This is discussed in more detail in the Appendix.

The mean correlation times obtained using a single log-Gaussian distribution are shown in Figure 5 for the two homopolymers and each component in three blends. The temperatures at which $\tau_{c_0} \simeq 2/\delta$ are estimated from the minimum in solid echo intensity as a function of temperature. The mean correlation time at the minimum in solid echo intensity is denoted by $\tau_{c,min}$. For dPVE, $\tau_{c,min} \simeq 16\ \mu s$, and for dPI, $\tau_{c,min} \simeq 26\ \mu s$; this difference is due to the fact that for dPI $\tau_{c,min}$ represents the log-weighted average of methyl and backbone deuterons, with 3 methyl deuterons having $2/\bar{\delta} \simeq 54\ \mu s$ and 5 backbone deuterons having $2/\delta \simeq 16\ \mu s$. These data are also included as distinct symbols in Figure 5 (+) and appear to be consistent with the 2D NMR data for the two homopolymers. Blends rich in PVE, however, exhibit mean correlation times estimated from 2D spectra that are substantially larger

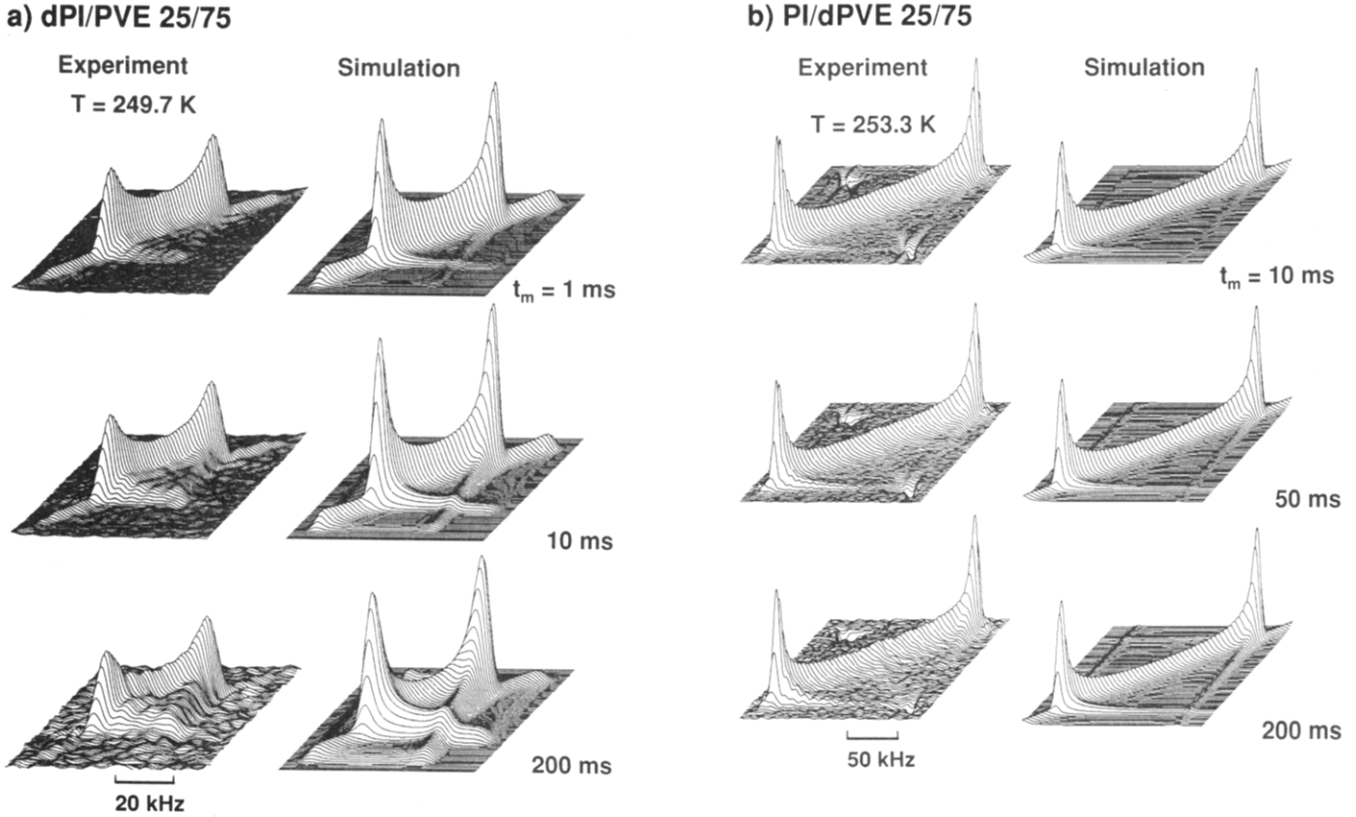

Figure 4. Experimental and simulated 2D ^{2}H exchange NMR spectra of the two components in 25/75 PI/PVE blends: (a) 25/75 dPI/PVE at 249.7 K (τ_{c_0} = 33 ms and σ = 1.85 decades); (b) 25/75 PI/dPVE at 253.3 K (τ_{c_0} = 1.33 s and σ = 1.75 decades).

than those obtained from the minimum in solid echo intensity. The deviation is particularly noticeable in 50/50 and 25/75 PI/PVE blends. This increase in the deviation appears to be related to the broad correlation time distribution and can be ascribed to the inhomogeneous reduction of signal in the intermediate dynamic regime (see Appendix).

To assess the effect of signal loss in the intermediate dynamic regime, solid echo intensities and the transverse NMR relaxation time (T_2) have been measured as a function of temperature (Figure 6). Since the detection of the signal in the five-pulse 2D exchange NMR experiment is done by solid echo, the loss of solid echo intensity gives rise to a similar loss of signal in the 2D exchange NMR experiment. The intensities in Figure 6a are normalized by the Boltzmann factor determining the temperature dependence of the spin population and scaled with the intensity obtained well below the glass transition. The decrease in solid echo intensity with temperature can be explained by two mechanisms: the change in T_2 relaxation times (Figure 6b), and incomplete echo formation due to changes in resonance frequency during the solid echo sequence.[33,36] Both mechanisms give rise to a correlation-time dependent reduction of spectral intensity, which is strongest at $\tau_c \simeq 2/\delta$.[32,37] Therefore, the 2D ^{2}H NMR spectra obtained near the glass transition of systems with a broad distribution of motional rates tend to underrepresent the most mobile segments whose mobilities lie in the intermediate dynamic regime. This leads to an overestimation of the mean correlation times and an underestimation of the width of the correlation time distribution. The effect of the loss of spectral intensity on the apparent correlation time distribution is discussed in more detail in the Appendix.

By taking this loss of signal into account in a semiquantitative way, the values of the corrected mean and width of the correlation time distribution, τ_c* and σ*, consistent with the observed 2D spectra and solid echo intensity can be estimated. The resulting values of τ_c* are shown as filled symbols (Figure 5). The temperature dependence of the correlation times for each pure component appears to be consistent with its established Williams–Landel–Ferry (WLF) behavior,

$$\log(\tau_{c_0}(T)) = \log \tau_g - \frac{C_1^g(T - T_g)}{C_2^g + (T - T_g)} \qquad (2)$$

where log τ_g is the mean correlation time at T_g, C_1^g and C_2^g are conventional WLF parameters, and T_g is the glass transition temperature (dashed curves Figure 5). For the literature values of WLF parameters C_1^g and C_2^g and the DSC T_g, reasonable WLF curves are obtained with log[τ_g (s)] $\simeq$ 0. The mean correlation times of PI and PVE in all three blends are also compared with a WLF temperature dependence as shown by the dashed curves, where the WLF parameters for each species are assumed to be independent of composition. The agreement is reasonable when the effect of intensity loss is approximately taken into account (filled symbols). The restricted WLF fit of the correlation times with fixed values of C_1^g and C_2^g renders different $T_g(\phi)$ for each species.

The different $T_{g,i}(\phi)$'s for each species i obtained from the restricted WLF fit describe the significant differences in their average mobilities. The difference in the mean correlation times between the two components close to the macroscopic T_g increases from 1.5 to more than 2 orders of magnitude as the PVE content increases. Alternatively, when we compare the $T_{g,i}(\phi)$ obtained from the fit, $T_{g,PVE} - T_{g,PI}$ increases from about 8 K for 75/25 PI/PVE to 15 K for 25/75 PI/PVE. This increased difference in mobilities between the two species with increasing PVE content is in accord with the more pronounced thermorheological

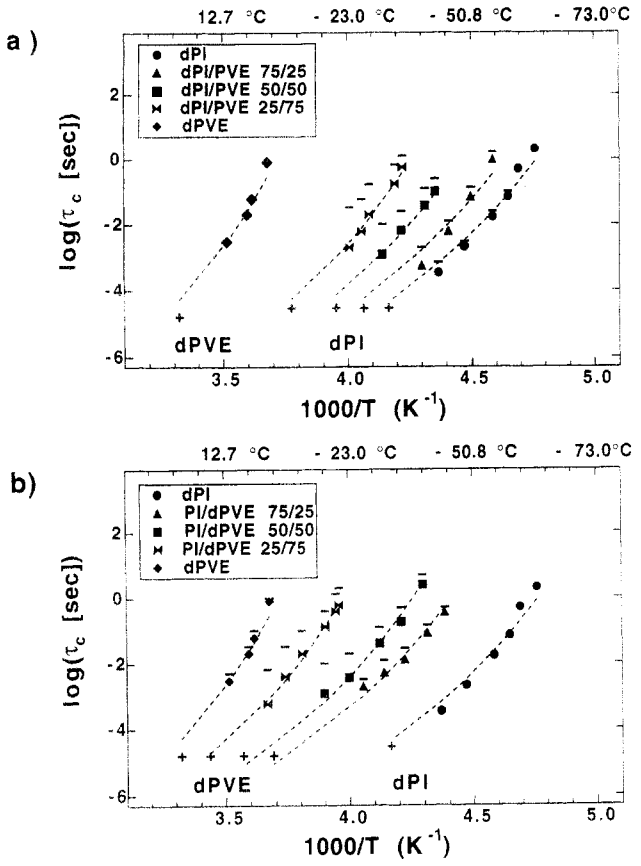

Figure 5. Apparent log-mean correlation times (horizontal dashes) as a function of temperature obtained from 2D spectra of (a) dPI and (b) dPVE and corrected log-mean correlation times (filled symbols) after taking into account the effect of the correlation time dependent reduction in spectral intensity. The + symbols are the mean correlation times estimated from the intensity and T_2 minima. The dashed lines are WLF curves for a rough qualitative comparison, obtained by using the WLF parameters C_1^g and C_2^g in the literature.[9] For dPI homopolymers, $C_1^g = 11.7$, $C_2^g = 52.9$ K, and $T_g = 210.4$ K. For dPVE, $C_1^g = 11.4$, $C_2^g = 56$ K, and $T_g = 270.6$ K. The WLF parameters C_1^g and C_2^g are assumed to be independent of composition. The $T_g(\phi)$'s obtained from the fit are nearly the same as the effective T_g shown in Table 1.

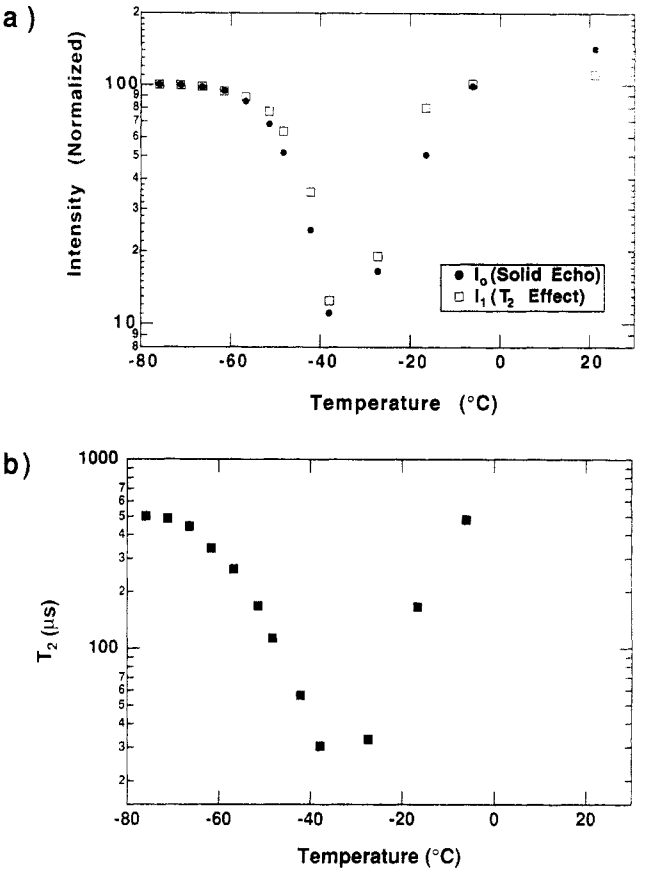

Figure 6. (a) Normalized solid echo intensity of dPI as a function of temperature and the estimated decay of the signal intensity due to the change in T_2 relaxation time. (b) The apparent T_2 relaxation time appears to exhibit a minimum where intensity becomes minimum.

complexity observed in blends rich in PVE.[38] This observation suggests that thermorheological complexity is directly related to differences in segmental mobilities of individual species near the glass transition.

Another quantity of interest is the width of the log-Gaussian distribution, σ, which is related to the distribution of mobilities and can be obtained from the fit of 2D NMR spectra. In previous literature, 2σ is often used as the full width of the correlation time distribution.[16,30] The full widths of the correlation time distributions (2σ) are shown in the Appendix (Figures 12 and 13), represented as vertical bars to $\pm\sigma$ from the mean correlation times. The widths (σ^*) that are obtained by taking the intensity loss into account are also presented similarly. As previously observed in the 50/50 PI/PVE blends and other homopolymers,[3,16,30] σ increases with decreasing temperature near T_g. The magnitude of σ at comparable values of τ_{c_0} exhibits a strong compositional dependence. Specifically, 75/25 PI/PVE blends show σ's that are comparable to those of homopolymers, whereas blends richer in PVE exhibit significantly increased σ's. Therefore, the broad glass transition of 75/25 PI/PVE is dominated by the difference in the mean mobilities between the two species, while the anomalously broad glass transitions for the 50/50 and 25/75 PI/PVE blends arise from both the separation in the mean mobilities and the broad distribution of mobilities for each species.

In contrast to the significant differences in the mean mobility, however, the σ's obtained at a common temperature appear to be quite close for both components at all compositions examined. It is inferred from this similarity in σ, despite the wide differences in τ_{c_0}, that the broadening of dynamics for both components arises from some structural heterogeneities that are shared by both species. The effect of purely statistical composition variation that was examined previously for the 50/50 PI/PVE blend is extended in the next section for blends at all compositions.

4. Discussion

4.1. Composition Dependence of Individual Glass Transition Temperatures. In many glass-forming systems, the glass transition is accompanied by sharp changes in viscosity and relaxation times as well as thermodynamic properties (heat capacity, thermal expansion coefficient, etc.).[39] A consistent definition of the glass transition temperature can be given in terms of certain relaxation times. For example, the temperature at which the macroscopic enthalpy relaxation time reaches $\simeq 100$ s can be defined as the glass transition temperature and is known to be correlated with the conventional onset temperature observed in a DSC measurement.[39] Although this definition of T_g seems consistent for many small molecular glasses and pure polymers, it becomes ambiguous for miscible blends in which the two components can exhibit widely different mobilities, even though the blend as a whole shows a single glass transition. In a 50/50 PI/PVE

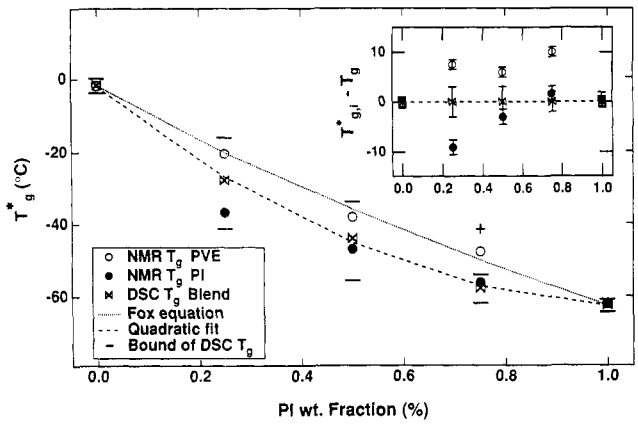

Figure 7. Composition dependence of the individual effective glass transition temperatures, T_g^*. The – symbols show the conventional upper and lower bounds of the glass transition determined by the tangent method. The + shown for the 75/25 PI/PVE blend corresponds to the upper bound of the DSC glass transition with the weak shoulder of heat capacity change taken into account (see Figure 8). The differences between the T_g^* and the DSC T_g are also displayed (inset).

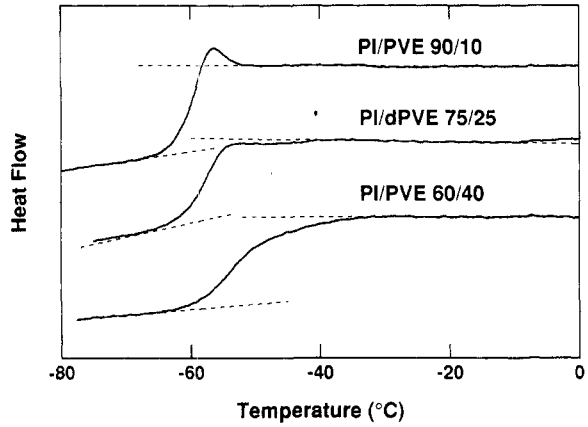

Figure 8. DSC traces for PI-rich blends. As the PVE fraction increases, the DSC traces show the development of the weak high-temperature shoulder.

blend, for example, the mean reorientation correlation times of the two components can differ by more than an order of magnitude. Therefore, it seems reasonable to define an effective glass transition temperature, T_g^* for individual species based on mean correlation times. Here, we define T_g^* as the iso-correlation-time temperature at which τ_{c_0} reaches 1 s. It can be obtained conveniently from the WLF fit of the correlation times by requiring $\log[\tau_g\ (s)] = 0$.

The T_g^*'s obtained from the corrected mean correlation times (filled symbols in Figure 5) are plotted against the PI weight fraction in Figure 7. The T_g^*'s are almost identical to the conventional DSC T_g for both pure components. In the blends, the T_g^*'s for the two components differ by more than 10 K, and the difference increases with increasing PVE fraction. However, the two individual T_g^*'s fall well within the DSC glass transition, except that the T_g^* of PVE in the 75/25 PI/PVE blend appears to fall outside the main glass transition. However, close inspection of the DSC traces for blends with high PI fraction (Figure 8) reveals that there is indeed a distinct but weak shoulder at temperatures corresponding to the T_g^* of PVE. This shoulder is also present in the DSC traces of other workers.[9,40]

The component T_g^*'s show different compositional dependences from each other and from the macroscopic DSC T_g. In particular, the difference between the DSC T_g and the T_g^* of PVE is nearly constant, at least for the compositions studied here, while the differences for PI go through a weak maximum and decrease almost monotonically with increasing PVE content (Figure 7, inset). This implies that the dynamics in miscible blends near the glass transition cannot be characterized solely in reference to the macroscopic T_g of the blend. When the mobility ratio of the two components obtained at various compositions is compared at temperatures with fixed $T - T_g$, the ratio varies with composition. For the particular choice of T_g based on the conventional calorimetric glass transition (Figure 7), the ratio of mobilities between PVE and PI would exhibit a distinct maximum near the PI weight fraction of 25%. Similar behaviors have been observed by tracer diffusion,[10] chain relaxation,[14] and segmental motions manifested in T_1 NMR relaxation times.[41] This often complicates the diffusion studies in miscible blends because the compositional dependence of tracer diffusivities due to the change in matrix glass transition cannot be compensated by simply shifting the measurement temperature with respect to the blend T_g. Significant discrepancies between the experimental and theoretical studies on the compositional dependence of the monomeric friction coefficient of each species seem to be related to this complex glass transition behavior.[10,14,15]

When we compared the T_g^* with simple empirical relations for the compositional dependence of T_g, we notice that the T_g^* of PVE agrees roughly with the Fox–Flory relation, while the T_g^* of PI increases close to linearly at PI fractions higher than 50%. Further studies are required to determine whether or not this behavior is typical in miscible blends with weak interactions.

4.2. Failure of Time–Temperature Superposition. The thermorheologically complex behavior observed in a number of miscible blends[8,9] can be explained in terms of a distinct temperature dependence of the monomeric friction coefficient, $\zeta_{0,i}$, where i indexes each component. In our previous paper,[3] a qualitative analogy between the $\zeta_{0,i}$ and $\tau_{c_0,i}$ was invoked to understand the failure of time–temperature superposition. It was demonstrated that the distinct $T_{g,i}^*$ underlying the broad DSC glass transition can describe the different temperature dependence of $\tau_{c_0,i}$ and, perhaps, $\zeta_{0,i}$. Here, the $\tau_{c_0,i}$ are directly compared with $\zeta_{0,i}$ obtained from the same set of polymer blends using simultaneous mechanical and birefringence measurements[38] (Figure 9). The two sets of data are compared quantitatively by introducing one adjustable constant for each pure component, which accounts for the ratio of $\zeta_{0,i}/T$ to τ_{c_0}. The connection is made using the general relationship between the shortest Rouse relaxation time of species i, $\tau_{R,i}$, and its friction coefficient, $\zeta_{0,i}$:

$$\tau_{R,i} = \frac{A_i}{k_B T}\zeta_{0,i} \tag{3}$$

where $A_i = a_i^2/3\pi^2$, a_i is the length of a Rouse chain segment, and $k_B T$ is the thermal energy. For comparison purposes, the value of A_i is adjusted so that the pure component data for both $\tau_{R,i}$ and $\tau_{c_0,i}$ can be best described by a common WLF fit. The same values of A_i are used for species i in the blends as well. The dotted lines shown in Figure 9 are the common WLF fits, and the parameters are listed in Table 1, where $\log[\tau_g\ (s)]$ is fixed to be 0, consistent with the definition of T_g^*. For the WLF curves shown in Figure 9, C_1^g is also fixed for each species, since we expect the extrapolated mobility at infinite temperature to be controlled by intrachain dynamic constraints, independent of composition. Furthermore, both C_1^g and

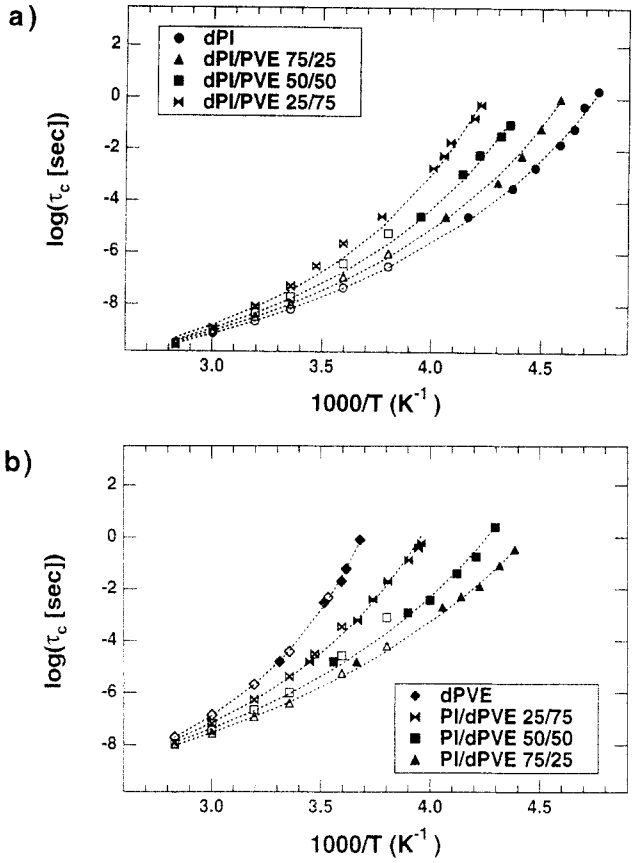

Figure 9. Comparison of τ_{c_0} and ζ_0 for each component in the same blend. The solid symbols are the same mean correlation times as shown in Figure 5, and the open symbols are the shortest Rouse-like relaxation time τ_R evaluated from the monomeric friction, ζ_0. The (-) symbols correspond to the mean correlation times from 2D spectra. The dotted lines are the best fit WLF curves that pass through both the τ_{c_0} and τ_R, and the parameters are listed in Table 1.

C_2^g cannot be determined unambiguously, within the experimental uncertainties. The proportionality factor A_i's determined empirically from $\tau_{c_0,i}k_BT/\zeta_{0,i}$ are much smaller than A_i directly calculated from the literature values of the statistical segment lengths. This is consistent with the fact that the segmental motion observed by ^2H NMR is more local than the Rouse chain dynamics.

The common WLF curves can describe both sets of data reasonably well over 8 decades of dynamic range for both homopolymers. For a given species i in a blend, $\tau_{R,i}$ and τ_{c_0} can roughly be described by a common WLF fit. As suggested previously,[3,9] the failure of time–temperature superposition can be described in terms of the different temperature dependences of the component dynamics. Though the dominant feature still seems to be the distinct individual T_g*, the other two parameters (C_1^g and C_2^g) also appear to have a weak compositional dependence, in spite of the similarity between these parameters for each pure component. Although experimental uncertainties limit our ability to quantitatively determine C_1^g and C_2^g, it is impossible to achieve a reasonable fit if they are both held fixed, independent of composition.

Although a common WLF curve approximately describes both rheological and NMR data for a given species in a blend, some deviations are evident, particularly in blends that have very broad correlation time distributions (*i.e.*, in 50/50 and 25/75 PI/PVE blends as evident in Figures 12 and 13). For the 50/50 and 25/75 PI/PVE blends, the rheological results for $\tau_{R,i}$ (open symbols) rise more strongly with decreasing temperature than the common WLF fit does. A WLF fit to the rheological data alone would lie above the mean correlation times, τ_{c_0}, but within the distribution of correlation times observed by NMR (see Figures 12 and 13). The NMR measurement probes segmental motions that correlate well with the monomeric friction coefficient in homopolymers. However, the rheological measurements probe ζ_0, which represents an average of segmental mobilities out to the scale of the entanglement molecular weight. Therefore, the systematic discrepancies between the temperature dependence of $\tau_{R,i}$ and τ_{c_0}, evidenced most strongly in blends with particularly broad distributions of τ_{c_0}, suggest that the species' ζ_0 measured rheologically may be a biased average of locally heterogeneous friction coefficients. This behavior is perhaps related to the way that the heterogeneity in segmental dynamics is propagated to the chain dynamics at a Rouse or reptation level.

4.3. Effect of Statistical Composition Variation. In this section the effect of statistical variation in composition previously discussed for a 50/50 blend[3] is extended to examine the compositional dependence of segmental dynamics. The effect of compositional variation on the mean and width of the correlation time distribution is calculated based on a simplistic model and is compared with experimental results.

In a real system, the dynamics of a test segment would depend on its intramolecular dynamic constraints and on the coupling of its dynamics with its neighbors. It is expected that the dynamics of a test segment would be strongly coupled to its neighbors, both because of connectivity along its backbone and because its neighbors are densely packed around it. Near the glass transition temperature, in particular, it has been speculated that the dynamic coupling extends much beyond the nearest neighbors.[42] This qualitative feature can be captured by treating the dynamics of a test segment as coupled to all the neighboring segments lying within a critical radius r_c. In this simple model, we represent this dynamic coupling by a local glass transition within a critical radius r_c. In the presence of local composition variations, this simple physical picture predicts a distribution of local glass transitions and hence a distribution of motional rates. The difference in average motional rates between the two components in a blend can also arise, since the test segment biases the composition of a local volume around it toward that of the test chain. This simple model is useful in showing how much of the observed broadening and difference in mobility between the two species can be ascribed to random variations in the local composition. The effects of *intrinsic* differences in the dynamics between the two species are not included in the model (*i.e.*, differences in dynamic coupling or intramolecular barriers to conformational rearrangement). When these are neglected, it turns out that this simple model cannot explain both the observed mean mobility difference and the width of the species' mobility distributions simultaneously.

In a blend of "A" and "B" with very weak interactions ($\chi \simeq 0$), one can assume that the neighbors of a particular chain are chosen randomly. The composition of its neighbors within the radius r_c has some distribution about the macroscopic composition. Thus, the composition of a subvolume is biased toward that of the test chain, since the test chain occupies a certain fraction of the subvolume due to connectivity and the rest of the subvolume is filled by either A or B randomly. The compositional distribution of the neighbors is approximated to be Gaussian, with mean equal to the macroscopic fraction of A, ϕ, and

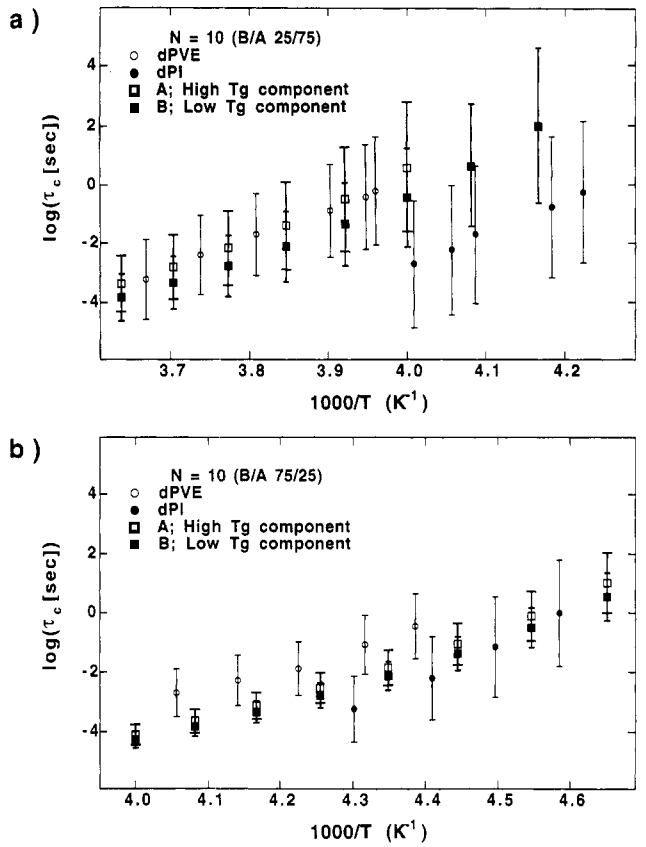

Figure 10. Mean and width of the correlation time distribution from the experiment (circles) and from the model calculation (squares) for a subvolume size of $N = 10$ (a) for 25/75 PI/PVE and (b) for 75/25 PI/PVE.

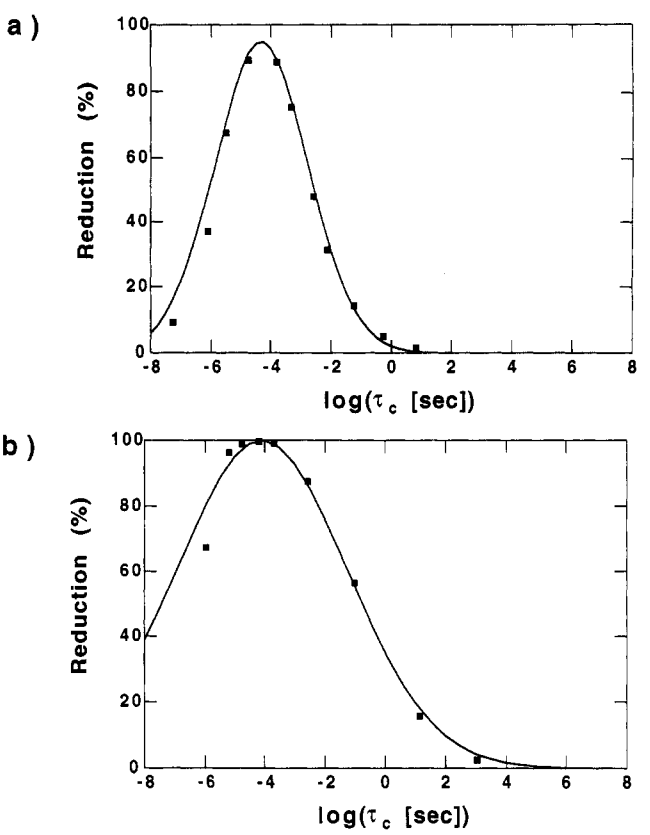

Figure 11. Average reduction of solid echo intensity as a function of mean correlation time for each homopolymer (a) dPI and (b) dPVE. The Gaussian fit through the data is used as the correlation time dependent reduction $\bar{R}_i(\tau_c)$ for each species i.

Table 1. WLF Parameters That Best Fit both the τ_{c_ϕ} and τ_R in Figure 9

species	composition (PI/PVE)	C_1^g	C_2^g (K)	T_g^* (K)
PI	100/0	12.85	49.6	210.9
	75/25	12.85	49.7	216.8
	50/50	12.85	46.9	226.3
	25/75	12.85	44.8	236.5
PVE	75/25	12.3	68.0	225.3
	50/50	12.3	65.4	234.4
	25/75	12.3	57.5	252.7
	0/100	12.3	48.6	271.2

variance, σ^2, estimated from the statistics of Bernoulli trials.[3]

The size of the region that influences the dynamics naturally affects the distribution of local composition; as r_c decreases, the number of neighboring units within the critical radius decreases and the variance of local composition increases. To connect this distribution of composition with the distribution of motional rates, one must adopt some method of mapping composition to mobility. Here, the approach suggested by Fischer and co-workers is taken.[43] The local compositional distribution is mapped into the local T_g distribution, using the compositional dependence of the macroscopic $T_g(\phi)$. The WLF temperature dependence of motional rates is used to calculate the distribution of motional rates of a test species. The details of their model and the procedures used to compute the distribution of motional rates have been discussed previously.[3]

The calculation and the experimental results are compared in Figure 10. For uniformity and ease of comparison, we designate A to be the high-T_g component (PVE) and B the low-T_g component (PI). In the calculation, the width of the correlation time distribution is governed by the mapping of variations in composition onto mobility distributions through the compositional dependence of the local $T_g(\phi)$. The size of the normalized critical radius $N = 2r_c/b$ (where b is the characteristic monomer/statistical segment size) is chosen to capture the observed broadening of T_g and the correlation time distribution for the 50/50 blend. The model does not account for the width of the correlation time distribution in the homopolymers; not surprisingly, in the 75/25 PI/PVE blend, in which the distribution width is comparable to that of the homopolymers, the model underpredicts the distribution width.

For the value of N that best reproduces the width of the correlation time distribution, the separation between the mean motional rates of A and B is much smaller than the experimental difference at all compositions. The separation between the mean motional rates would increase if the bias in the composition of each subvolume is increased. This could be achieved by reducing the subvolume size so the test chain occupies a larger fraction of it. However, increasing the bias in composition toward the test chain makes the σ's of the two species differ significantly, since σ for a high-T_g species becomes substantially larger as a result of the increasing sensitivity of mobility as the fraction of high-T_g component, ϕ, increases. This behavior implies that the observed segmental dynamics cannot be completely explained by local compositional variation alone. The remaining differences in the mean correlation times between the two species are likely due to the intrinsic dynamic differences between the two species.

5. Conclusion

We have measured, using 2D ^{2}H NMR, the dramatic change in segmental mobilities of two species in miscible blends as a function of composition. As the content of the high-T_g component (PVE) increases, the difference be-

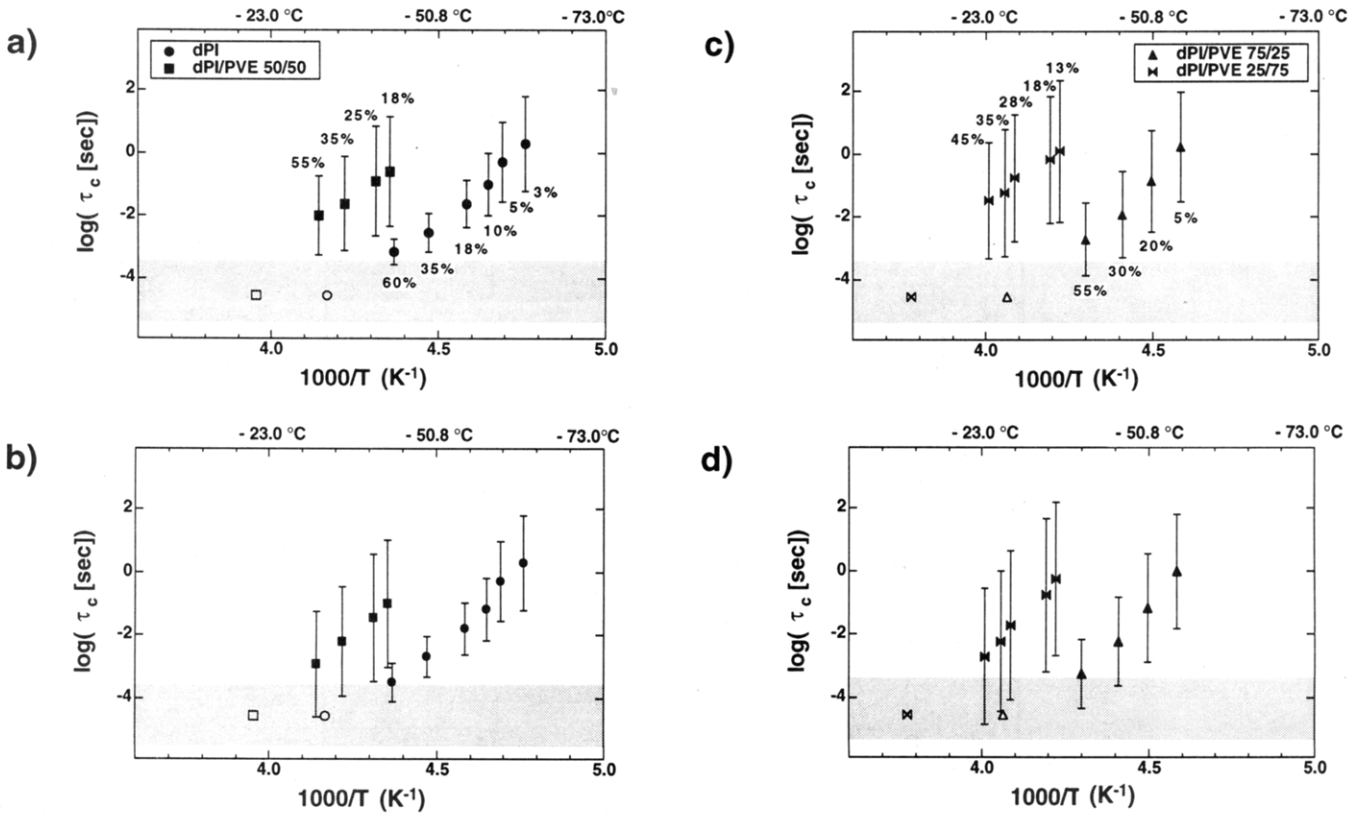

Figure 12. Effect of reduction on the determination of the mean and width of the correlation time distribution of PI: (a and c) apparent mean τ_{c_0} (symbol) and width σ (vertical bars corresponding to $\pm\sigma$) without accounting for intensity reduction $\bar{R}$ (percent reductions observed from solid echo measurement are indicated); (b and d) modified mean τ_c* and width of the correlation time distribution σ* in accord with the observed τ_{c_0}, σ, and $\bar{R}$. The shaded area corresponds to the range of correlation times that undergo more than 80% reduction. Open symbol corresponds to the mean correlation times obtained from the intensity/T_2 mininum. Parts a and b are for pure dPI and 50/50 dPI/PVE blend; parts c and d are for 25/75 and 75/25 dPI/PVE blends.

tween the mean motional rates of the two species increases. These differences can be described in terms of separate effective glass transition temperature, $T^*_{g,i}$, for each species i, whose difference increases with PVE content. The growing difference between the individual T_g*'s may explain the more pronounced thermorheological complexity observed for high PVE fraction in these blends. The individual T_g*'s also show different compositional dependences from each other and from the macroscopic DSC T_g. As the relative difference between $T_{g,PVE}^* - T_g$ and $T_g - T_{g,PI}^*$ changes, the mobilities observed at a given $T - T_g$ vary significantly. Thus, viewing the dynamics with respect to the macroscopic T_g can give rise to a complex nonmonotonic dependence on composition.

Similarly, the width of the mobility distribution increases for both species as the content of high-T_g component (PVE) increases. This behavior can originate from random composition variations. Based on a simplistic model, local composition variations can give rise to the observed broadening of the mobility distribution. The broadening is pronounced when the glass transition temperature changes rapidly with composition, which is often the case in blends rich in the high-T_g species. Although this model can explain the observed σ and its composition dependence, the observed differences in the mean mobilities cannot be explained simultaneously. This may be due to the intrinsic dynamic differences between the two species, which are neglected in the simplistic model. Both the broadening of the correlation time distribution and the significant differences in mean motional rates give rise to the changes in the width of the glass transition in miscible blends.

Acknowledgment. We gratefully acknowledge the support of the National Science Foundation Presidential Young Investigator Award (J.A.K.), Chevron, the Caltech Consortium in Chemistry and Chemical Engineering, du Pont de Nemours, Eastman Kodak, and the Petroleum Research Fund, administered by the American Chemical Society.

6. Appendix

6.1. Reduction of NMR Spectral Intensity. When the solid echo intensity is measured as a function of temperature, it exhibits a broad minimum at about 30 K above the glass transition. This behavior has been observed in many systems and has also been used to determine the nature of segmental dynamics in a number of polymer systems.[31,32,37,44] This reduction of signal is often described in terms of a minimum in the effective T_2 relaxation time and/or the incomplete refocusing of the magnetization (Figure 6). Both effects appear to have a strong dependence on correlation time, with the reduction becoming strongest at $\tau_c \simeq 2/\delta$. Although this reduction of signal is most intense in the intermediate dynamic regime ($1\ \mu s \leq \tau_c \leq 1$ ms), some reduction is observed over a very wide range of correlation times. The reduction is significant, even in the temperature range where 2D NMR spectra are obtained. Thus, it is possible that the correlation time distribution determined from 2D spectra is biased toward slower motions, since the correlation-time dependent reduction is stronger for C–^{2}H bonds lying in the fast tail of the actual correlation time distribution. We suggest an approximate procedure, based on solid echo intensity measurements, to correct for the effect of correlation time dependent reduction of spectral intensity.

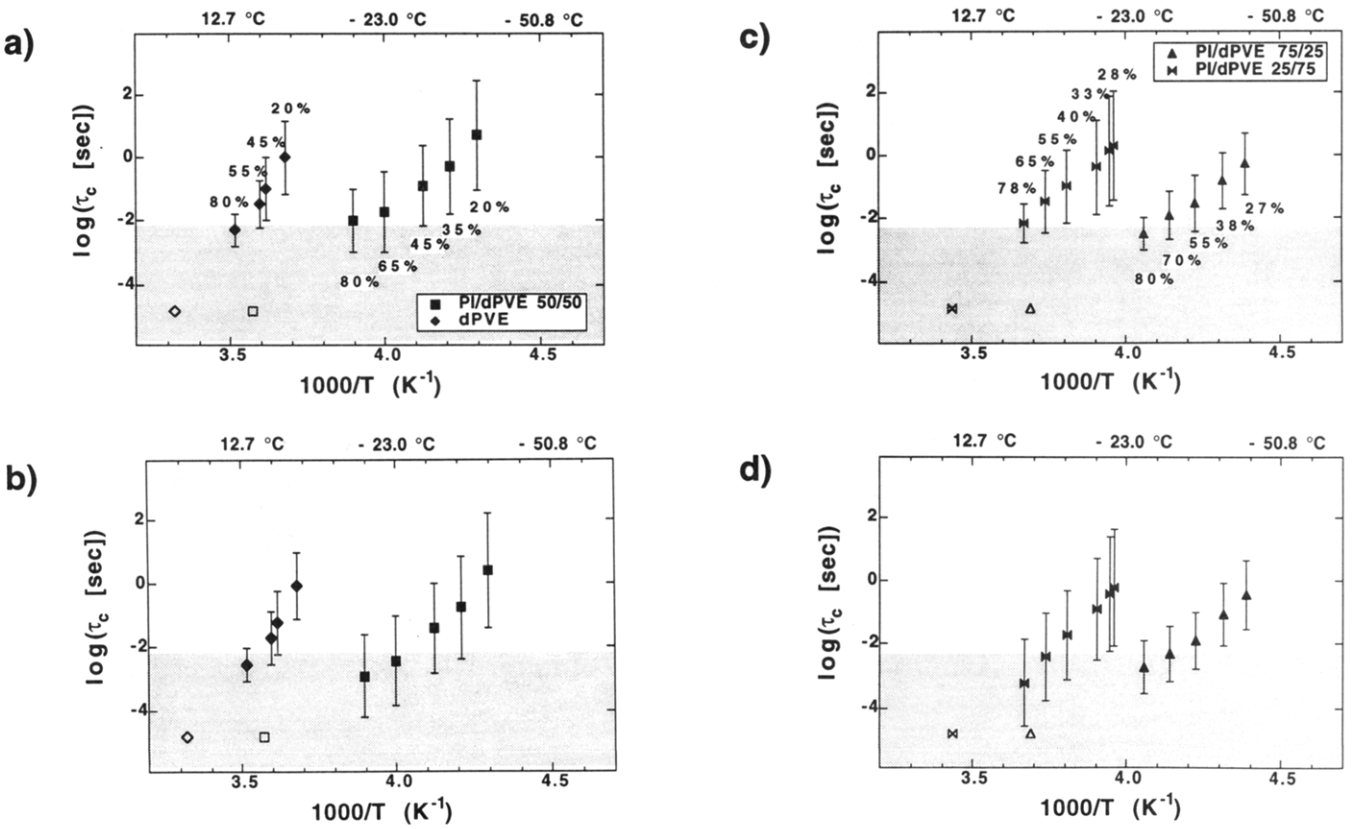

Figure 13. Apparent correlation time distribution (τ_{c_0},σ) obtained from the experimental 2D spectra of dPVE (a and c) and the modified distribution (τ^*_c,σ^*) obtained by accounting for the effect of correlation time dependent reduction (b and d). (See Figure 12 for symbol code.)

The reduction of spectral intensity at a single correlation time, $R(\tau_c)$, can, in principal, be obtained from a detailed calculation of the solid echo spectrum as a function of a single correlation time τ_c.[31,32] Alternatively, this relationship between the reduction and the correlation time can be approximately obtained by measuring the average reduction as a function of temperature, $\bar{R}_i(T)$, for each species i. For two homopolymers, the inherent correlation time distribution is relatively narrow, and it is expected that the measured average reduction over the distribution of correlation times, $\bar{R}_i(\sigma,\tau_{c_0};T)$ is similar to the reduction at the mean correlation time $R_i(\tau_{c_0};T)$. The temperature dependence of the mean correlation times, $\tau_{c_0,i}(T)$, is used to obtain $R_i(\tau_c)$ from the measured reduction $\bar{R}_i(T)$ for each species i. The continuous representation of the correlation time dependent reduction is obtained by approximating the measured reduction as a Gaussian function (Figure 11).

Once we have $R_i(\tau_c)$, we can calculate the effect of the correlation-time dependent reduction on the apparent correlation time distribution determined from the 2D NMR spectra. Suppose the actual underlying correlation time distribution is $P_i^*(\tau_c;\phi,T)$; then the apparent correlation time distribution $P(\tau_c;\phi,T)$ can be evaluated via

$$P(\tau_c;\phi,T) = (1 - R(\tau_c))\, P^*(\tau_c;\phi,T) \tag{4}$$

and the average reduction $R_i(\phi,T)$ is given by

$$\bar{R}(\phi,T) = \frac{\int [P^*(\tau_c;\phi,T) - P(\tau_c;\phi,T)]\, d\tau_c}{\int P^*(\tau_c;\phi,T)\, d\tau_c} \tag{5}$$

Now, we want to estimate the mean and width of the actual correlation time distribution based on the experimentally measured quantities, which are the apparent mean and width of the correlation time distribution determined from the 2D NMR spectra and the average reduction measured by solid echo intensity measurement. As a first approximation, we assume that the actual correlation time distribution can be represented as a log-Gaussian distribution,

$$P^*(\tau_c) = \frac{\exp[-(\log \tau_c - \log \tau_c^*)^2/2\sigma^{*2}]}{(2\pi\sigma^{*2})^{1/2}} \tag{6}$$

where $\tau_c^* = 10^{\langle \log \tau_c \rangle}$ is the log-mean correlation time and σ^* is the width of the correlation time distribution. $P^*(\tau_c)$ is then subjected to reduction via eq 5. The set of values (τ_c^*,σ^*) are taken as the modified mean and the width of the correlation time distribution, when the average reduction, the apparent mean, and the variance of the correlation time distribution after the reduction are consistent with the observed $\bar{R}$, τ_{c_0}, and σ. The $\bar{R}$, τ_{c_0}, and σ obtained experimentally are compared with the τ_c^*,σ^* determined by the correction procedure outlined above (Figures 12 and 13). The modified mean correlation time is also included in Figures 5 and 9. The range of correlation times that undergo more than 80% reduction is also shaded to facilitate comparison. The difference between (τ_{c_0},σ) and (τ_c^*,σ^*) is most pronounced for the PVE-rich blend, where the correlation time distributions are very broad.

When the width of the correlation time distribution is sufficiently broad, this reduction of intensities can also give rise to an apparent bimodality, as previously observed by other workers.[44] This apparent bimodality is manifested most dramatically by the presence of a central peak, while the rest of the 2D spectrum still exhibits a solid line shape (Figure 14a). The bimodality in the correlation time distribution, however, disappears at lower temperatures,

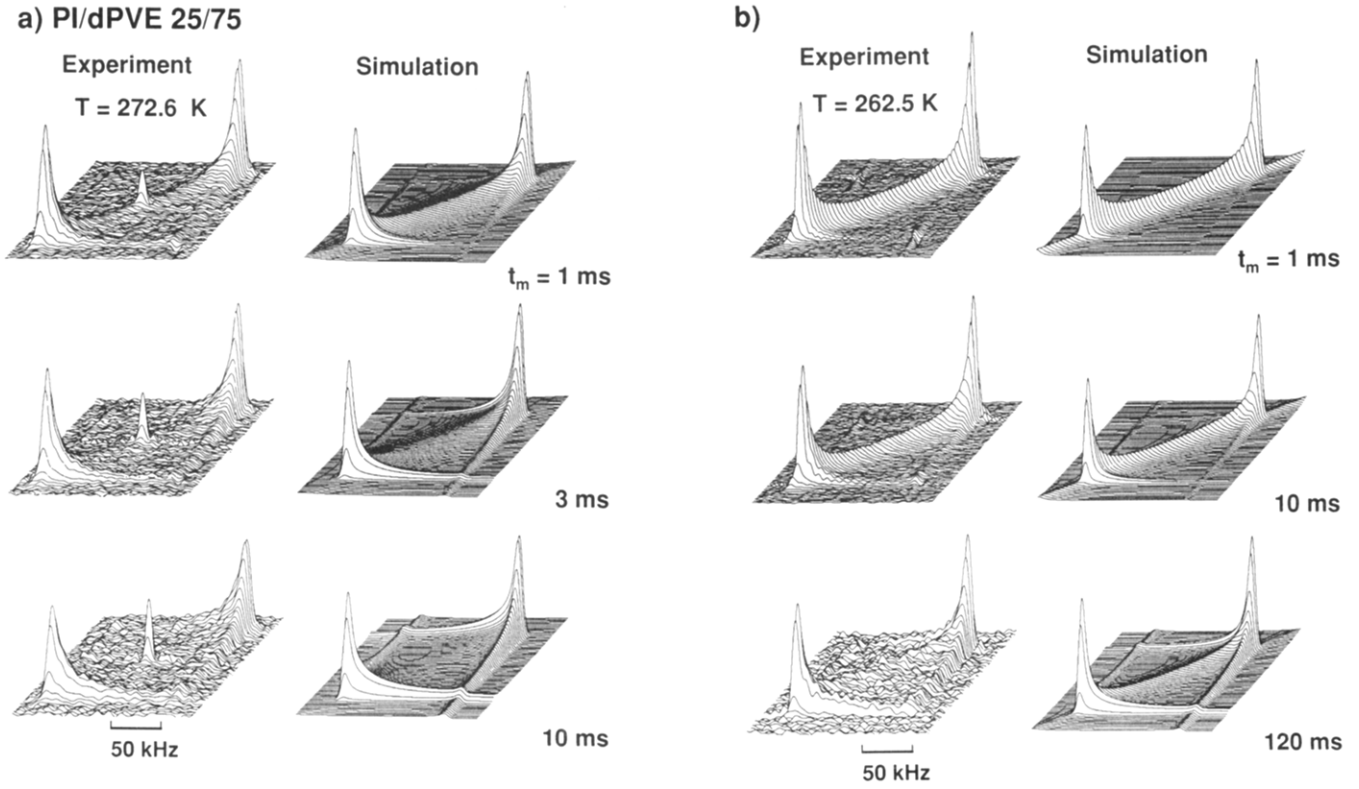

Figure 14. A series of 2D ^{2}H exchange NMR spectra for 75/25 PI/dPVE. Simulated spectra are obtained from a unimodal log-Gaussian correlation time distribution. (a) Spectra obtained at 272.6 K. The presence of the isotropic peak at the center of the spectra is due to the components with $\tau_c \leq 10^{-5}$ s. This seemingly bimodal character can be explained by the loss of signal occurring predominantly at the intermediate dynamic regime. Simulated spectra are calculated with τ_{c_0} = 6.7 ms and σ = 0.625 decade. The narrow isotropic peak is neglected in the fit, but it would account for about 2% of the observed intensity. This is in accord with the estimate based on the apparent correlation time distribution arising from a single unimodal correlation time distribution due to the reduction in intensity (see Figure 15 and text). (b) Spectra obtained at 262.5 K. Simulated spectra are calculated with τ_{c_0} = 100 ms and σ = 1.15 decades. Also see Figure 4b for corresponding spectra at 253.3 K. The spectra taken at 253 K, 262 K, and intermediate temperatures do not show the existence of a distinctly fast component.

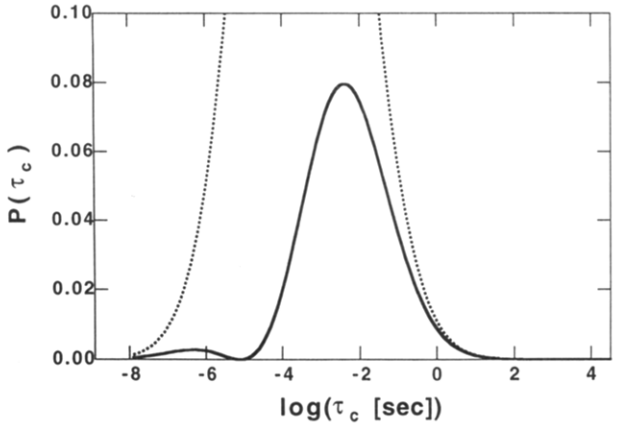

Figure 15. Apparent bimodal distribution resulting from the loss of spectral intensity at the intermediate dynamic regime. The dotted line is the actual underlying correlation time distribution that is consistent with the measured τ_{c_0},σ, and average reduction of signal $\bar{R}$. The peak height of the dotted line is about 0.295 and is truncated to emphasize the bimodal character of the solid curve. The apparent bimodal correlation time distribution emerges as a consequence of the correlation time dependent reduction of the NMR spectral intensity.

as can be seen from the absence of the fast segments that give rise to a significant exchange even at small mixing times (Figure 14). This qualitative change in the shape of the correlation time distribution can be demonstrated by using the above scheme of correcting for the effect of reduction at the intermediate dynamic regime (Figure 15). The apparent bimodality can arise from a single log-Gaussian distribution of correlation times (dotted line), due to the reduction of exchange intensity at the center of the actual correlation time distribution (solid line). The narrow central peak arises from the small tail at high correlation time ($\tau_{c_0} \leq 10^{-6}$).

References and Notes

(1) Prest, W. M.; Porter, R. S. *J. Polym. Sci., Part A-2* **1972**, *10*, 1639.
(2) (a) Chin, Y. H.; Inglefield, P. T.; Jones, A. A. *Macromolecules* **1993**, *26*, 5372. (b) Chin, Y. H.; Zhang, C.; Wang, P.; Inglefield, P. T.; Jones, A. A.; Kambour, R. P.; Bendler, J. T.; White, D. M. *Macromolecules* **1992**, *25*, 3031.
(3) Chung, G.-K.; Kornfield, J. A.; Smith, S. D. *Macromolecules* **1994**, *27*, 964.
(4) Lodge, T. P. *J. Chem. Phys.* **1993**, *97*, 1480.
(5) Lau, S.; Pathak, J.; Wunderlich, B. *Macromolecules* **1982**, *15*, 1278.
(6) Lin, J. L.; Roe, R. J. *Polymer* **1988**, *29*, 1227.
(7) Zetsche, A.; Kremer, F.; Jung, W.; Schulze, H. *Polymer* **1990**, *31*, 1883.
(8) Colby, R. H. *Polymer* **1989**, *20*, 1275.
(9) Roovers, J.; Toporowski, P. M. *Macromolecules* **1992**, *25*, 3454.
(10) (a) Composto, R. J.; Kramer, E. J.; White, D. M. *Macromolecules* **1988**, *21*, 2580. (b) Composto, R. J.; Kramer, E. J.; White, D. M. *Polymer* **1990**, *31*, 2320.
(11) Schneider, H. A.; Brekner, M. J. *Polym. Bull.* **1985**, *14*, 173.
(12) Gordon, J. M.; Rouse, G. B.; Gibbs, J. H.; Risen, W. M. *J. Chem. Phys.* **1977**, *66*, 4971.
(13) Couchman, P. R. *Macromolecules* **1991**, *24*, 5772.
(14) Zawada, J. A.; Ylitalo, C. M.; Fuller, G. G.; Colby, R. H.; Long, T. E. *Macromolecules* **1992**, *25*, 2896.
(15) Meire, G.; Fytas, G.; Momper, B.; Fleischer, G. *Macromolecules* **1993**, *26*, 5310.
(16) Pschorn, U.; Rössler, E.; Sillescu, H.; Kaufmann, S.; Schaefer, D.; Spiess, H. W. *Macromolecules* **1991**, *24*, 398.
(17) Tomlin, D. W.; Roland, C. M. *Macromolecules* **1992**, *25*, 2994.
(18) Roland, C. M. *Macromolecules* **1987**, *20*, 2557.

v(19) Roland, C. M. *J. Polym. Sci., Polym. Phys. Ed.* **1988**, *26*, 839.
(20) Roland, C. M.; Miller, J. B.; McGrath, K. J. *Macromolecules* **1993**, *26*, 4967.
(21) Roovers, J.; Wang, F. *J. Non-Cryst. Solids*, in press.
(22) The DSC measurements are reproduced after standard low-temperature calibration with mercury and show deviation from the previous report[3] by about 4 K at the glass transition of the pure components.
(23) Carella, J. M.; Graessley, W. W.; Fetters, L. J. *Macromolecules* **1984**, *17*, 2775.
(24) Schmidt, C.; Wefing, S.; Blümich, B.; Spiess, H. W. *Chem. Phys. Lett.* **1986**, *130*, 84.
(25) Schmidt, C.; Blümich, B.; Spiess, H. W. *J. Magn. Reson.* **1988**, *79*, 269.
(26) Jelinski, L. W. *High Resolution NMR Spectroscopy of Synthetic Polymers in Bulk*; Komoroski, R. A., Ed.; VCH Publishers: Deerfield Beach, FL, 1986.
(27) Schaefer, D. Ph.D. Thesis, University of Mainz, 1992.
(28) Kaufmann, S.; Wefing, S.; Schaefer, D.; Spiess, H. W. *J. Chem. Phys.* **1990**, *93*, 197.
(29) Wefing, S.; Kaufmann, S.; Spiess, H. W. *J. Chem. Phys.* **1988**, *89*, 1234.
(30) Schaefer, D.; Spiess, H. W. *J. Chem. Phys.* **1992**, *97*, 7944.
(31) Spiess, H. W.; Sillescu, H. *J. Magn. Reson.* **1981**, *42*, 1981.
(32) Woessner, D. E.; Snowden, B. S.; Meyer, G. H. *J. Chem. Phys.* **1969**, *51*, 2968.
(33) Rössler, E.; Sillescu, H.; Spiess, H. W. *Polymer* **1985**, *26*, 203.
(34) Powles, J. G.; Strange, J. H. *Proc. Phys. Soc. London* **1963**, *82*, 6.
(35) Chung, G.-C. Ph.D. Thesis, California Institute of Technology, 1994.
(36) The apparent T_2 relaxation time is obtained using the solid echo pulse sequence and measuring the change in the echo amplitude as a function of duration of the echo. Since this experiment is based on the solid echo experiment, the measured echo amplitude is reduced not only due to the effective T_2 relaxation but also due to an incomplete refocusing close to the intermediate dynamic regime. Therefore, the effect of the T_2 relaxation process cannot be completely separated from the effect of incomplete refocusing.
(37) Schmidt, C.; Kuhn, K. J.; Spiess, H. W. *Prog. Colloid Polym. Sci.* **1985**, *71*, 71.
(38) (a) Arendt, B. A.; Kannan, R. M.; Zewail, M.; Kornfield, J. A.; Smith, S. D. *Rheol. Acta* **1994**, *33*, 322. (b) Arendt, B. A.; Krishnamoorti, R.; Kornfield, J. A.; Smith, S. D. T., to be published.
(39) Angell, C. A. *J. Non-Cryst. Solids* **1991**, *131–133*, 13.
(40) The relative magnitude of the heat capacity change at the high-temperature shoulder is about 10% or less of the total, which is much less than the PVE weight fraction. This can be partially accounted for by the relative magnitude of the heat capacity change at the glass transition of the two pure components (PI shows about 50% more heat capacity change than PVE). Furthermore, a broad hump similar to that observed for the 90/10 PI/PVE blend may also be present with a smaller magnitude in the actual changes in heat capacity for the 75/25 blend. This may have affected the appearance of the DSC trace and hence reduce the apparent heat capacity changes at the high-temperature shoulder.
(41) Le Menestrel, C.; Kenwright, A. M.; Sergot, P.; Laupretre, F.; Monnerie, L. *Macromolecules* **1992**, *25*, 3020.
(42) Adam, G.; Gibbs, J. H. *J. Chem. Phys.* **1965**, *76*, 139.
(43) Fischer, E. W.; Zetsche, A. *Polym. Prepr. (Am. Chem. Soc., Div. Polym. Chem.)* **1992**, 78.
(44) Wehrle, M.; Hellmann, G. P.; Spiess, H. W. *Colloid Polym. Sci.* **1987**, *265*, 815.